Smart Home Energy Management with Mitigation of Power Profile Uncertainties and Model Errors

Rémy Rigo-Mariani, Arif Ahmed

Smart Home Energy Management with Mitigation of Power Profile Uncertainties and Model Errors

Rémy Rigo-Mariani[a,b], Arif Ahmed[c]

a Université Grenoble Alpes, CNRS, Grenoble INP, G2Elab, F-38000 Grenoble, France

b CNRS@CREATE, 1 Create Way, Singapore

b Energy and Power Systems Group, TUMCREATE Ltd., 1 Create Way, Singapore

ARTICLE INFO

Keywords:

Smart Home
Energy Management
Model Predictive Control
Thermal Model
Uncertainties Mitigation
Optimization

ABSTRACT

The paper proposes a two-stage home energy management system accounting for optimal energy dispatch, power profiles predictability, and building thermal behaviour. The first look-ahead stage aims at minimizing the energy exchanges with the upstream grid based on load and weather predictions. The second step adapts the controls in real-time in order to mitigate forecast errors while remaining as close as possible to the look-ahead commitments. The originality of the paper lies on the use of different granularities of the building models. Especially, this allows to account for the approximations in the system equations embedded in the predictive controllers. Furthermore, a real-time tuning of those model equations is performed based on the deviations observed on the state variables – errors between controller predictions and measurements. Ultimately the proposed approach allows to cope with two generic drawback of traditional model predictive control: *i)* environment forecast errors and *ii)* models approximations. Several simulations are carried out to under different weather conditions, demonstrating an average energy exchange reduction of at least 25% and better system predictability. The work is completed with sensitivities analysis of the controller settings, the system parameters and the quality of weather/load forecasts.

Below is the nomenclature of the main used symbols in the proposed management strategy:

Sets :

$t \in T$	set of time steps (time step *dt* in hour)

Variables :

p_t^{bat+}, p_t^{bat-}	charge/discharge power of battery at time *t* (kW)
soc_t	battery state of charge at time *t* (%)
u_t^{bat+}	battery in charging mode at time *t* {0,1}
p_t^{gd}	grid power at time *t* (kW)
p_t^c, p_t^h	HVAC cooling/heating power at time *t* (kW)
p_t^{hc}	HVAC power at time *t* (kW)
u_t^c	HVAC in cooling mode at time *t* {1,0}
T_t^s	Temperature setpoint at time *t* (°C)

Parameters:

p_t^l, p_t^{pv}	load and solar generation at time *t* (kW)
T_t^a	ambient temperature at time *t* (°C)
G_t	solar radiation (W/m²)
a_c^{Ts}, a_c^{Ta}, b_c	HVAC model coefficient in cooling mode (kW/°C, kW)
a_h^{Ts}, a_h^{Ta}, b_h	HVAC model coefficient in heating mode (kW/°C, kW)
$\overline{p^{bat}}, \overline{e^{bat}}$	battery rated power and capacity (kW, kWh)
soc_0	initial state of charge (%)
η	battery efficiency (-)
$.^*$	superscript to denote the committed profiles
Δp^{gd}	Tolerance bandwidth around committed grid power (kW)
Δsoc	Tolerance bandwidth around *soc* profile (%)
ΔT	Tolerance bandwidth around committed temperature (°C)

1 Introduction

Over the past decades, the necessity to cope with limited fossil fuels and the need for reduced carbon emissions led to the increasing penetration of renewable based energy sources in power and energy systems [1]. Especially, greater numbers of systems are connected at the end-users levels, behind-the-meter, consisting then in small-scale units widely spread over the distribution networks [2]. Such renewable-based distributed energy resources (DERs) allows reduced system losses with generation closer to the points of consumption and reduced energy bills for the users – higher ratios of self-consumption and self-sufficiency [3]. More efficient performances can be achieved when considering other types of DERs – as battery storage systems [4] , fuel cells [5] or local

generation units [6] – for a better match between the local generation and consumption. At the building or household level, it is possible to uptake more flexibilities and reach higher energy efficiency while actively controlling appliances (e.g. shiftable loads) [7]. Another possibility is to account for thermal comfort constraints and make use of the buildings, thermal inertia as additional storage capabilities [8] - considering the Heating Ventilation and Air Conditioning (HVAC) system, its consumption and its impact on the house temperature. Indeed, such multi-energy approaches allow the best performances while taking advantage of the interaction between energy carriers and their respective demand – performances can be further enhanced while considering combined heat and power units and/or thermal storages [5].

In order to enable the aforementioned system performances, Energy Management Strategies (EMS) have long been investigated in the framework of smart grid and renewable energy integration for small-scale systems such as 'smart homes' [8]. Those management schemes typically rely on Model Predictive Control (MPC) where the DERs setpoints are computed based on prediction of the system environment (i.e. load/generation profiles) and models of the system itself – i.e. potentially including the model of the building/household when thermal comfort is considered [5] [7] [9]. In most cases the control takes the form of a cost-driven optimization (i.e. minimization of the energy bill [9] [10] [11]), with potential environmental objectives such as carbon emissions [12], [13], and/or technical criteria - e.g. Peak to Avera Ratio (PAR) of the power profile exchanged with the upstream grid [7], [13]. Deterministic optimizations are then performed on a look-ahead basis, typically along a 24 h window and the considered algorithms depend on the type of models considered. Mixed Integer Linear Programming (MILP) is widely used, especially when binary variables/constraints are necessary to account for the operation of shiftable/interruptible load (i.e. on/off status) [9], [10], [14]. Mixed Integer Non-Linear Programming (MINLP) is applied when nonlinearities occur in the modeling of storage degradation [15], electrical grid [13], or HVAC system [16]. Heuristics [17] and metaheuristics as genetic algorithms [12] or particle swarm optimization [11] are also used when multi-objectives or strong nonlinearities are considered.

Most of the studies previously commented refer to MPC run in a somewhat single stage in the sense that the control performances are assessed in an offline mode assuming perfect forecast. In actual implementations, uncertainties of renewable generation and/or load profile degrade the performances of the controller. Redispatching and adaptive strategies, closer to real-time (typically at the resolution of some minutes), are then necessary to cope with uncertainties and well-identified MPC shortcomings [18]. Two-stage management can then be considered with near real-time phases that consider updated forecasts for power and/or price profiles [6]. Another potential of two-stage approaches is that they can allow two mitigate uncertainties from the upstream grid perspective and thus improve both its operational and long-term planning [6]. In practice, the near real-time phase adapts the actual controls so that the power profile at the house level (i.e. grid power profile) remains as close as possible to a scheduled predefined in the look-ahead phase. This can be done through the use of fast heuristics [19], [20] or traditional MILP [21], [22].

Mitigation of forecast errors has since been noticeably investigated – load/generation prediction, energy prices, and/or environmental factors such as ambient temperature or solar radiation. However, MPC approaches also suffer from a lack of perfect accuracy of the models embedded in the controllers. Indeed, most of the equations are convex in order to avoid prohibitive computational times of the MPC. Due to those model approximations, the actual system may not respond accordingly to the predictions. It is then deemed important to assess the performances of the proposed controls after they are sent to the system, which is not done in any of the aforementioned references. Validation on more accurate building models (e.g. EnergyPlus software) can still be found in the literature while applying reinforcement learning [23], [24] or traditional MILP [25] for cost reduction. Some studies with experimental results on real-life systems over a sample of actual rooms [26] or an entire house [27]. However, the proposed management strategies focus on cost reduction with comfort constraints with no real-time correction to mitigate power profile uncertainties.

This paper then investigates a two-stage home energy management and takes advantage of different model granularities in order to validate the controls on a system that is mathematically different from the equations embedded in the MPC controllers. The first stage based on traditional MILP aims at minimizing the energy exchanges with the main electrical grid. This objective is deemed more generic than traditional cost reduction criteria that depend on the countries, and power providers. The second stage (based either on MILP or a heuristic)

allows to adapt the controls in order to stick to the committed profiles following the first look-ahead stage and while mitigating load/generation uncertainties. Also, the models in the near real-time controls are adapted online based on the observed deviations between the predicted system state values and the measurements. This allows to assess and improve the performances of the proposed controls once they are sent to a validation model (i.e. more accurate). Appendix B summarizes the paper scope with regards to the investigated references and the main contributions of the paper are as follows:

- A two-stage management strategy to reduce energy exchanges and enhance system predictability at a household level – > 25 % fewer exchanges compared to a baseline scenario.
- The consideration of different model granularities to compensate for the lack of accuracy of model-based controllers and real-time tuning of the models based on observed deviations. Ultimately, the proposed management allows to mitigate both forecast errors and model approximations for predictive control.
- The simulation/validation of the proposed approach over different controller settings, and system parameters while accounting for different weather/load forecast qualities.

2 Building Model Granularities

2.1 Controlled System

The considered case study accounts for the thermal behavior of the system while considering the electricity needed for heating/cooling with respect to the ambient temperature (T_t^a), solar irradiation (G_t,) and numerous building parameters. Ultimately, for a given electrical load value (p_t^l) and solar generation (p_t^{pv}), the electrical power exchanged with the grid (p_t^{gd}) is impacted by the two degrees of freedom in the system – i.e. the battery charge/discharge powers (p_t^{bat+},p_t^{bat-}) and the zone temperature setpoint set by the user (T_t^s) that impacts the electrical load for heating/cooling (p_t^h/p_t^c). Figure 1 displays the generic layout of the single-house system behind the meter. Note that the weather conditions, which are inputs for simulation, embed the solar radiation (G_t) that is used (with the ambient temperature T_t^a) to compute the generated solar power (p_t^{pv}) based on a standard single-diode solar model [28].

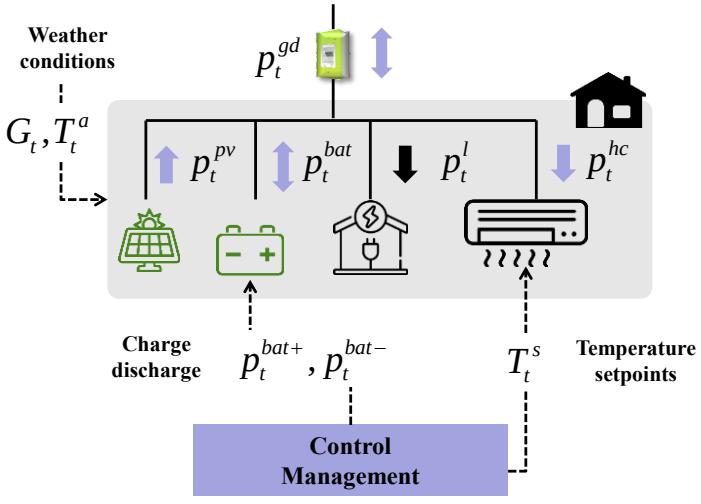

Figure 1: Controlled system

2.2 Building Thermal Models

2.2.1 Reference Model

As previously mentioned, the simulation accounts for the thermal behavior of the house/building by modeling the dynamic thermal nature of the house/building and considering the impact of HVAC power for heating (p_t^h) and cooling (p_t^c). A reference system model is then established based on prior works carried out in the context of multi-energy system modeling [29]. The model serves as a reference to evaluate the HVAC

electrical power required for heating/cooling and output corresponding dynamic zone temperature (T_t^z) of the house/building. The house/building model equations embed major building characteristics such as its surface/volume, orientation, widow area, the thermal resistance of walls, etc. For numerical stability purposes, an internal time resolution of one minute is set for the house/building model simulation. The heating/cooling HVAC power is then estimated based on the weather conditions – i.e. ambient temperature and solar radiation while accounting for the orientation of the walls with regard to the solar position, and the zone temperature setpoint (T_t^s). The zone temperature setpoint is a user-defined controllable input, which serves to fulfill the temperature comfort level inside the house/building. The zone temperature setpoint here is considered as an actual degree of freedom in the system control and a PID controller is added to the original model equations in order to adapt the heating/cooling power based on measured errors between the actual zone temperature (T_t^z) and the reference setpoint (T_t^s). Various time-varying parameters from the reference system model are then used as inputs to a lower resolution (e.g. 5 min and 30 min) model that depends on the control horizon. Figure 2 summarizes the input/outputs of the considered reference system model, detailed equations can be referred to in the documentation on prior projects [29], and are not presented here as it is outside the scope of the paper.

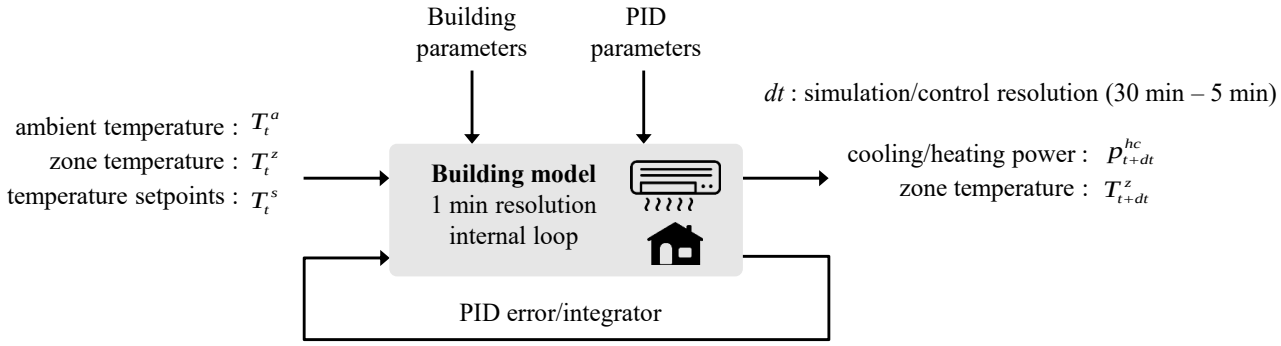

Figure 2: Reference Model for the building thermal behavior.

2.2.2 Simplified Models

The energy management strategy proposed in this paper is based on model predictive control (MPC). The equations of the original model, and especially the need for fine temporal resolutions, are not compatible with look-ahead approaches. Especially, considering fine resolutions over longer periods of time (e.g. day-ahead) in optimization-driven solutions leads to increased complexity and heavy computational burden. Thus, in our proposed approach, simplified HVAC power models are developed from the reference model based on least square minimization fitting and an experimental perturbation of the reference model with various temperature setpoints (in the range 18 °C – 24 °C), ambient temperature values (in the range -20°C – 40 °C), and initial room temperature (in the range 18 °C – 24 °C) to capture the dynamics of the reference system in the simplified model. More specifically, two distinct simplified HVAC power models are generated corresponding to the two control horizons considered that will be presented in the following section – i.e. a 30 min and a 5 min model for day-ahead and near real-time control, respectively. The first simplified HVAC power model at 30 min resolution is set up based on the linear dependency of the heating/cooling power with the temperature setpoint (T_t^s) and ambient temperature (T_t^a). At 30 min time steps, results showed that the average HVAC power depends marginally on the initial zone temperature provided that it is already controlled in the range corresponding to the desired setpoints – i.e. within 18 °C to 24 °C. For every investigated data sample in the fitting process, the original system model is run over a 30 min period with an internal one-minute resolution loop. A distinction is made whenever the system operates in cooling mode (i.e. temperature setpoints lower than ambient temperature) or heating (i.e. temperature setpoints higher than ambient temperature). This results in two sets of fitting coefficients for the 30 min resolution model in Eq. (1) (lower script '30'). Similarly, the fitting at 5 min resolution is performed with two distinct operating modes (cooling and heating). However, in this case, the initial zone temperature proved to have a significant impact on the average heating/cooling power over five minutes with different temperature setpoints and ambient temperature values. Thus, additional terms and coefficients relating to the zone temperature (T_t^z) are included in the fitting model in Eq. (2).

$$\begin{cases} p_t^c = a_{c30}^{T^a} \times T_t^a + a_{c30}^{T^s} \times T_t^s + b_{c30} \\ p_t^h = a_{h30}^{T^a} \times T_t^a + a_{h30}^{T^s} \times T_t^s + b_{h30} \end{cases} \quad (1)$$

$$\begin{cases} p_t^c = a_{c5}^{T^a} \times T_t^a + a_{c5}^{T^s} \times T_t^s + a_{c5}^{Tz} \times T_t^z + b_{c5} \\ p_t^h = a_{h5}^{T^a} \times T_t^a + a_{h5}^{T^s} \times T_t^s + a_{h5}^{Tz} \times T_t^z + b_{h5} \end{cases} \quad (2)$$

3 Energy Management Strategy

3.1 Two-Stage Control

The proposed energy management strategy consists of a two-stage approach with *i)* an optimization on a look-ahead phase that computes the predicted (commitment) grid power profile for the next day and *ii)* a near real-time correction of the controls in order to fulfill as much as possible the commitment i.e. minimize the deviation of actual power from the predicted power profile. Figure 3 describes the proposed methodology with both look-ahead and near real-time phases relying on the developed simplified models discussed in the previous section.

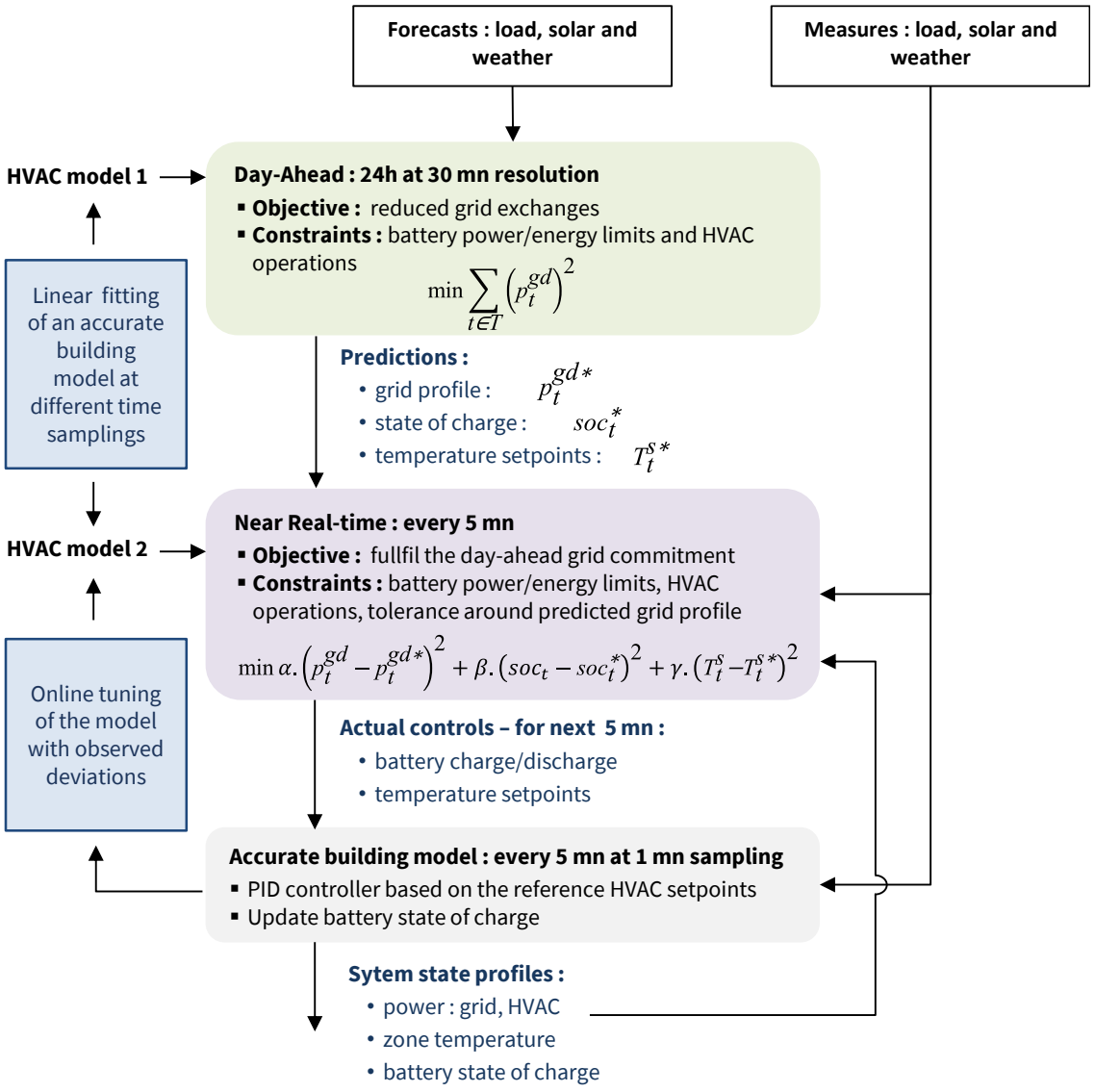

Figure 3: Flowchart of the proposed methodology.

All the outputs from the day-ahead phase denote the commitments (upperscript "*") in terms of predicted grid power profile (p_t^{gd*}), temperature setpoints (T_t^{s*}) and state of charge of the battery (soc_t^*). The near real-time stage minimizes the errors with those commitments with a set of weighting factors (α, β, γ) – priority is given to the errors with the committed grid power profile (α). The near real-time stage is run every 5 min and computes the controls ultimately sent to the system which is then simulated over the next time-step. As already mentioned, once the actual system is emulated, actual HVAC power is estimated and is used for online tuning of the model integrated into the 5 min MPC. (see section 2.4). The following subsections detail the operations of the successive phases.

3.2 Day-Ahead Commitment

The day-ahead stage consists of an MPC problem, which is based on forecasted values for the load (p_t^l), the generation (p_t^{pv}), and the ambient temperature (T_t^a). The main objective of the day-ahead stage is to generate the commitment grid power profile and schedules for the controls (i.e. battery charge/discharge and temperature setpoints) for the next 24 hours. This stage takes the form of an optimization problem whose objective function is to smooth the grid power profiles over the optimization window T (i.e. 24 hours here) (Eq. (3)). From the mathematical perspective, this continuously differentiable objective has the advantage of convexity. More importantly, from the user's point of view (i.e. the building/house owner), it allows to reduce at the same time the imported energy and the peak power which have the greatest impact on the electricity bill. Finally, for power system applications, this objective is somewhat representative of the losses minimization due to the line power flow and is also consistent with typical cost-driven optimizations that assume quadratic generation cost (i.e. increasing marginal costs in unit commitment problems [30]).

$$obj: \min \sum_{t \in T} \left(p_t^{gd} \right)^2 \tag{3}$$

The first set of constraints (Eq. 4 – Eq. 8) in the day-ahead problem refers to the operating limits for the battery in terms of power and energy (i.e. state of charge soc_t). Especially, bounds for charging/discharging p_t^{bat+}, p_t^{bat-} account for the battery rated power and operating mode with the binary variable u_t^{bat+}denoting the charging mode (Eq. (4) and Eq. (5)) in order to avoid simultaneous charging and discharging. Note that a traditional alternative formulation embeds two distinct binary variables for charging and discharging with an additional constraint to ensure that only one of the two is nonnull at every time step. It is not considered here for a reduced complexity of the problem and in order to reduce the solution time. The state of charge (soc_t) shall remain in the range 0-100 % (Eq. (6)) and is updated at every time step with the charge/discharge power according to the simplified linear model in Eq. (7). The model accounts for the battery efficiency η and nominal capacity ($\overline{e_{bat}}$). Additional constraint (Eq. (8)) allows to set the initial (soc_0) and final SOC values to be similar (typical cyclic constraint for energy conservation purposes). Note that for simplicity purposes, 'storage capacity' here denotes the 'usable capcity', which explains that the *soc* is allowed to varies in the range 0-100 %. This is the capacity purchased. In practice, the acual capacity is greater, and the battery management system controls the actual voltage and actual state of charge (typically never below 20 % for Li-Ion batteries).

$$0 \le p_t^{bat+} \le u_t^{bat+} \times \overline{p^{bat}} \quad \forall t \in T \tag{4}$$

$$0 \le p_t^{bat-} \le \left(1 - u_t^{bat+}\right) \times \overline{p^{bat}} \quad \forall t \in T \tag{5}$$

$$0 \le soc_t \le 100 \quad \forall t \in T \tag{6}$$

$$soc_{t+1} = soc_t + \left(p_t^{bat+} \times \eta - \frac{p_t^{bat-}}{\eta} \right) \times \frac{dt}{\overline{e^{bat}}} \times 100 \quad \forall t \in T \tag{7}$$

$$soc_{t=1} = soc_{t=\|T\|+1} = soc_0 \tag{8}$$

The next set of constraints relates to the simplified model to compute the HVAC power based on the temperature setpoints between the bounds in Eq. (9). Similar to the battery charge/discharge modes, cooling (p_t^c) and heating (p_t^h) cannot occur at the same time. This is ensured with constraint Eq. (10) and the use of the

binary variable u_t^c denoting that the system is operated in cooling mode with an upper limit theoretical ($\lambda = 10^6$). Cooling occurs whenever the ambient temperature (predicted) is greater than the temperature set points, and heating otherwise as ensured with Eq. (11). Constraints Eq. (12) and Eq. (13) computes the cooling/heating power of the HVAC with the fitting coefficients for the proposed linear model. The BigM method here ensures that the appropriate operation and power estimation is valid depending on the operating mode (binary variable value).

$$18 \le T_t^s \le 24 \quad \forall t \in T \tag{9}$$

$$\begin{cases} 0 \le p_t^c \le u_t^c \times \lambda \\ 0 \le p_t^h \le \left(1 - u_t^c\right) \times \lambda \end{cases} \forall t \in T \tag{10}$$

$$\begin{cases} T_t^a - T_t^s \le u_t^c \times \lambda \\ T_t^s - T_t^a \le \left(1 - u_t^h\right) \times \lambda \end{cases} \forall t \in T \tag{11}$$

$$\begin{cases} p_t^c \le a_{c30}^{T^a} \times T_t^a + a_{c30}^{T^s} \times T_t^s + b_{c30} + \left(1 - u_t^c\right) \times \lambda \\ p_t^c \ge a_{c30}^{T^a} \times T_t^a + a_{c30}^{T^s} \times T_t^s + b_{c30} - \left(1 - u_t^c\right) \times \lambda \end{cases} \forall t \in T \tag{12}$$

$$\begin{cases} p_t^h \le a_{h30}^{T^a} \times T_t^a + a_{h30}^{T^s} \times T_t^s + b_h + u_t^c \times \lambda \\ p_t^h \ge a_{h30}^{T^a} \times T_t^a + a_{h30}^{T^s} \times T_t^s + b_h - u_t^c \times \lambda \end{cases} \forall t \in T \tag{13}$$

Finally, the last constraint Eq. (14) refers to the overall power balance that ultimately sets the grid power value at every time step and depending on the different settings and operating modes for the flexible/controllable assets (i.e. HVAC and battery here) – with the HVAC power being the sum of cooling and heating powers. The optimal decisions are driven by the forecasted input profiles: ambient temperature (T_t^a), electrical load (p_t^l) and solar generation (p_t^{pv}). It should be noted that the solar generation prediction accounts for the expected ambient temperature and solar radiation. Also, note that the grid power is here an unbounded continuous variable that could be either positive or negative. There is no limitation (e.g. in terms of subscribed power) and no discrimination between import from or export to the grid (e.g. with distinct buying and selling prices of electricity [16]), as the operation is not cost-driven here (Eq. (3)). The optimization problem for this MPC over a daily horizon (at 30 min resolution) takes ultimately the form of a Mixed Integer Quadratic Programming problem (MIQP). The output predicted profiles (upperscript "*") are obtained from the optimization, which are the grid power (p_t^{gd*}), the battery state of charge (soc_t^*), and scheduled temperature setpoints (T_t^{s*}). These are further used in the subsequent real-time problem.

$$p_t^{gd} + p_t^{bat-} + p_t^{pv} = p_t^l + p_t^{bat+} + \underbrace{p_t^h + p_t^c}_{p_t^{hc}} \quad \forall t \in T \tag{14}$$

3.3 Near Real-time Correction

In near-real-time operation, the actual values for the load (p_t^l)., the solar power (p_t^{pv}) and ambient temperatures (T_t^{amb}) is expected to differ from the predictions. In this paper, the measured values in real-time display the same notations as the prediction in the day-ahead phase (i.e. T_t^a, p_t^l and p_t^{pv}) for the sake of clarity. It should be noted that the time resolution is not the same moving from 30 min in day-ahead to 5 min in near real-time control. Due to the unavoidable prediction errors, corrective actions shall then be taken in the operational phase in order to fulfill the commitment as much as possible. In other words, the objective is to remain close to the predicted grid profile $p_t^{gd*}$with a tolerance bandwidth Δp^{gd} while adjusting the controls at the current time step t – i.e. battery charge/discharge (p_t^{bat+}, p_t^{bat-}) and temperature setpoints (T_t^s). Similar to the previous phase, the near real-time operation relies on an MPC approach over a single time step. The objective is to penalize the deviations above the tolerance (p_t^{gd+}) and below (p_t^{gd-}) as shown in Eq. (15). Deviations regarding the battery state of charge and temperature setpoints are also considered with a set of weighting factors α (equal to10^6 for the priority given to the grid power correction), β (equal to10^3, second priority to temperature setpoints) and γ (equal

to 1). The main idea being to take advantage of the degree of freedom provided by the tolerance bandwidth on the grid power to realign the other variables – e.g. if the battery has been over-discharged at the previous time steps to mitigate past uncertainties, its SOC can be corrected if the necessity to shave a peak load that was predicted in the following minutes/hours. In addition, state of charge deviations can be constraints within a tolerance around the predicted profiles as in Eq. (16) – note that the computation of soc_t accounts for the actual SOC measurement and the update constraints that implicitly represents the storage model in Eq. (7), while the charge/discharge limits are still embedded with Eq. (4) and Eq. (5). Another operational constraint limits the variation of temperature setpoints with ramping bounds ΔT^s (Eq. (17)) while the overall power balance equation remains the same as Eq. (14) over the considered time step (and accounting for the actual measured values for load and solar generation).

$$obj: \min \alpha \times \left(p_t^{gd-} + p_t^{gd+}\right)^2 + \beta \times \left(T_t^s - T_t^{s*}\right)^2 + \gamma \times \left(soc_t - soc_t^*\right)^2 \quad (15)$$

$$\max\left(0, soc_t^* - \Delta soc\right) \le soc_t \le \min\left(100, soc_t^* + \Delta soc\right) \quad (16)$$

$$T_{t-1}^s - \Delta T^s \le T_t^s \le T_{t-1}^s + \Delta T^s \quad (17)$$

In addition to the constraints mentioned previously, the mathematical formulation of the real-time control problem shall handle the nonlinearity incurred by the need to quantify the grid power deviation beyond the tolerance bandwidth. As illustrated in Figure 4, this formulation requires the introduction of additional variables in order to discriminate the different cases. In practice, binary variables allow to identify if the grid power is above (u_t^{gd+}) or below (u_t^{gd-}) the tolerance bandwidth (Δp^{gd}) with constraint Eq. (18). Obviously, those two cases cannot occur simultaneously, which is ensured with Eq. (19). In order to quantify the deviations above the tolerances, two continuous variables are introduced p_t^{gd+}, p_t^{gd-} and are non-null whenever the corresponding binary variables u_t^{gd+}, u_t^{gd-} are active (i.e. = 1) (Eq. (20)). A last variable p_t^{gd0} is needed to capture any grid power values within the tolerance (Eq. (21)) while the overall relationship between the introduced quantities is driven by constraint Eq. (22) that reconstructs the expected grid power for the considered time step.

$$\begin{cases} p_t^{gd} - (p_t^{gd*} + \Delta p^{gd}) \le u_t^{gd+} \times \lambda \\ (p_t^{gd*} - \Delta p^{gd}) - p_t^{gd} \le u_t^{gd-} \times \lambda \end{cases} \quad (18)$$

$$u_t^{gd+} + u_t^{gd-} \le 1 \quad (19)$$

$$\begin{cases} 0 \le p_t^{gd+} \le u_t^{gd+} \times \lambda \\ 0 \le p_t^{gd-} \le u_t^{gd-} \times \lambda \end{cases} \quad (20)$$

$$p_t^{gd*} - \Delta p^{gd} \le p_t^{gd0} \le p_t^{gd*} + \Delta p^{gd} \quad (21)$$

$$p_t^{gd} = p_t^{gd0} + p_t^{gd+} - p_t^{gd-} \quad (22)$$

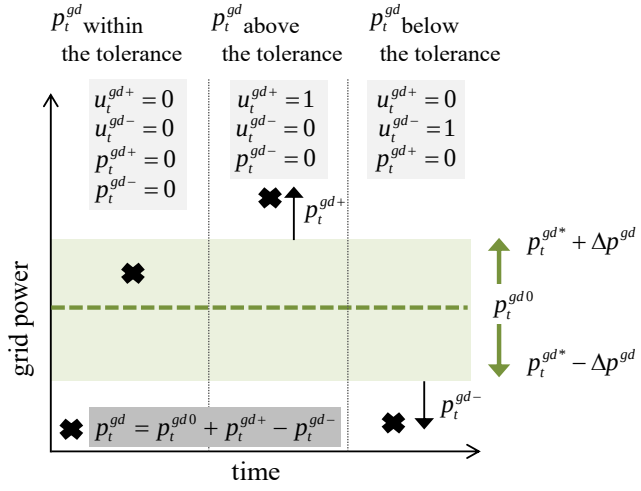

Figure 4: Additional variables and formulation to identify/quantify grid power deviation around the committed profile.

Similar to the day-ahead phase, the expected grid power values depend on the HVAC power estimated with a simplified least-square fit model of the building and the temperature setpoints values (i.e. degree of freedom). In near real-time operation, the thermal model accounts for the measured zone temperatures and the 5 min resolution fitting mentioned in Section 1.2.2. The formulation relies on the same approach as the one described for the look-ahead MPC with the binary variable u_t^c denoting that the system operates in cooling mode, and corresponding constraints on the setpoints and cooling mode detection (Eq. (9) – Eq. (11)). Constraints that estimate the HVAC power integrate the correct fitting coefficient and model formulation (Eq. (23) and Eq. (24)).

$$\begin{cases} p_t^c \le a_{c5}^{T^a} \times T_t^a + a_{c5}^{T^s} \times T_t^s + a_{c5}^{T^z} \times T_t^z + b_{c5} + \left(1 - u_t^c\right) \times \lambda \\ p_t^c \ge a_{c5}^{T^a} \times T_t^a + a_{c5}^{T^s} \times T_t^s + a_{c5}^{T^z} \times T_t^z + b_{c5} - \left(1 - u_t^c\right) \times \lambda \end{cases} \quad \forall t \in T \qquad (23)$$

$$\begin{cases} p_t^h \le a_{h5}^{T^a} \times T_t^a + a_{h5}^{T^s} \times T_t^s + a_{h5}^{T^z} \times T_t^z + b_{h5} + u_t^c \times \lambda \\ p_t^h \ge a_{h5}^{T^a} \times T_t^a + a_{h5}^{T^s} \times T_t^s + a_{h5}^{T^z} \times T_t^z + b_{h5} - u_t^c \times \lambda \end{cases} \quad \forall t \in T \qquad (24)$$

Both MPC stages (first MILP stage and second MIQP stage) are written in Matlab using YALMIP Toolkit [31] and solved with Gurobi.

3.4 Online Tuning of the Simplified Thermal Model

Decisions taken in near real-time then rely on an approximation of the thermal behavior – denoted $\tilde{p}_t^{hc}$ in this subsection – which is in practice the output from the MPC corresponding to the mathematical equations that represent the HVAC operations (i.e. contribution of cooling/heating powers). Once the controls are actually sent and processed by the system using the reference, the actual HVAC power can be accessed. Preliminary results display a very significant error between the actual HVAC power p_t^{hc} and the predicted $\tilde{p}_t^{hc}$ – 57 % Mean Average Error – MAE depicted in Figure 5a over a daily horizon. Thus, despite the very good determination factors (R^2 > 0.95) obtained with the fitting at 5 min resolution (Section 1.2.2), the simplified linear fitting model fails to capture the realistic behavior of the heating/cooling power, with respect to the temperatures (ambient, room and setpoints). This is due to the effect of the PID corrector in the actual building equations that adapts the HVAC power to comply with the temperature setpoints. Its effects are not captured in the model simplification as every sample considered in the fitting is generated with the PID error set to zero.

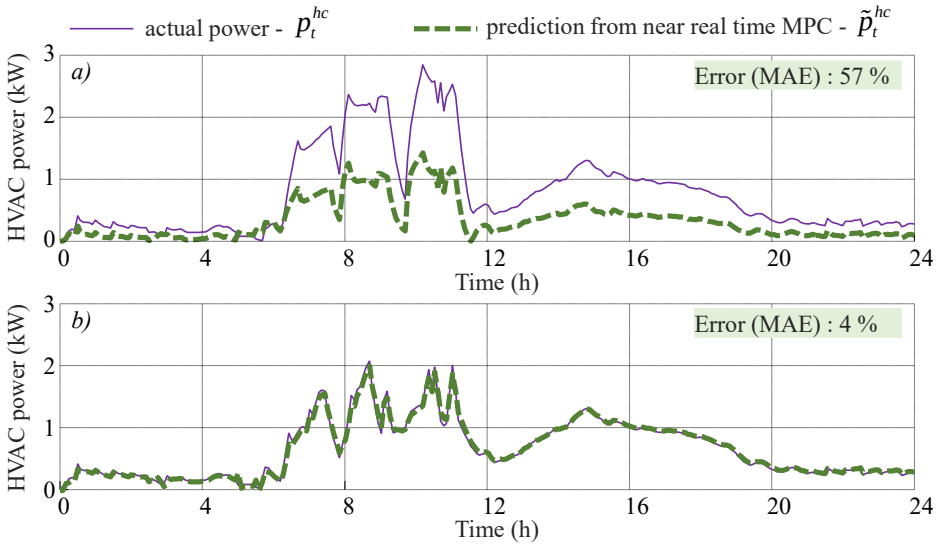

Figure 5: Real-time HVAC power simulated and predicted with 5 min resolution simplified model – a) without online correction of the simplified model – b) with online adaption of the simplified model.

Thus, the use of the 5 min resolution model is enhanced in this section by keeping track of the error between the model estimation and the measured values once the controls are processed and the system is simulated (Eq. (25)). Then equations Eq. (23) and Eq. (24) that estimate the cooling/heating power integrate this error as

an additional term in the simplified model (Eq. (26) and Eq. (27)). Ultimately, this allows to strongly reduce the error between the power estimated in the real-time MPC and the actual value (4 % Mean Average Error – MAE in Figure 5b), which will ultimately lead to a better control of the grid power profiles as discussed further in the results section.

$$e_t = e_{t-1} + p_t^{ht} - \tilde{p}_t^{ht} \tag{25}$$

$$\begin{cases} p_t^c \le a_{c5}^{T^a} \times T_t^a + a_{c5}^{T^s} \times T_t^s + a_{c5}^{T^z} \times T_t^z + b_{c5} + e_t + \left(1 - u_t^c\right) \times \lambda \\ p_t^c \ge a_{c5}^{T^a} \times T_t^a + a_{c5}^{T^s} \times T_t^s + a_{c5}^{T^z} \times T_t^z + b_{c5} + e_t - \left(1 - u_t^c\right) \times \lambda \end{cases} \quad \forall t \in T \tag{26}$$

$$\begin{cases} p_t^h \le a_{h5}^{T^a} \times T_t^a + a_{h5}^{T^s} \times T_t^s + a_{h5}^{T^z} \times T_t^z + b_{h5} + e_t + u_t^c \times \lambda \\ p_t^h \ge a_{h5}^{T^a} \times T_t^a + a_{h5}^{T^s} \times T_t^s + a_{h5}^{T^z} \times T_t^z + b_{h5} + e_t - u_t^c \times \lambda \end{cases} \quad \forall t \in T \tag{27}$$

3.5 Rule-Based-Controller for Near Real-time Operations

In a second step, a Rule-Based-Controller (RBC) is implemented for near real-time management. The main motivation is to be able to quickly provide a solution for the actual controller implementation and with ensured convergence. For simulation purposes, such RBC can also allow testing a wide range of setups as will be discussed in the following section – e.g. different installed capacities of the assets, impact of the forecast accuracy.

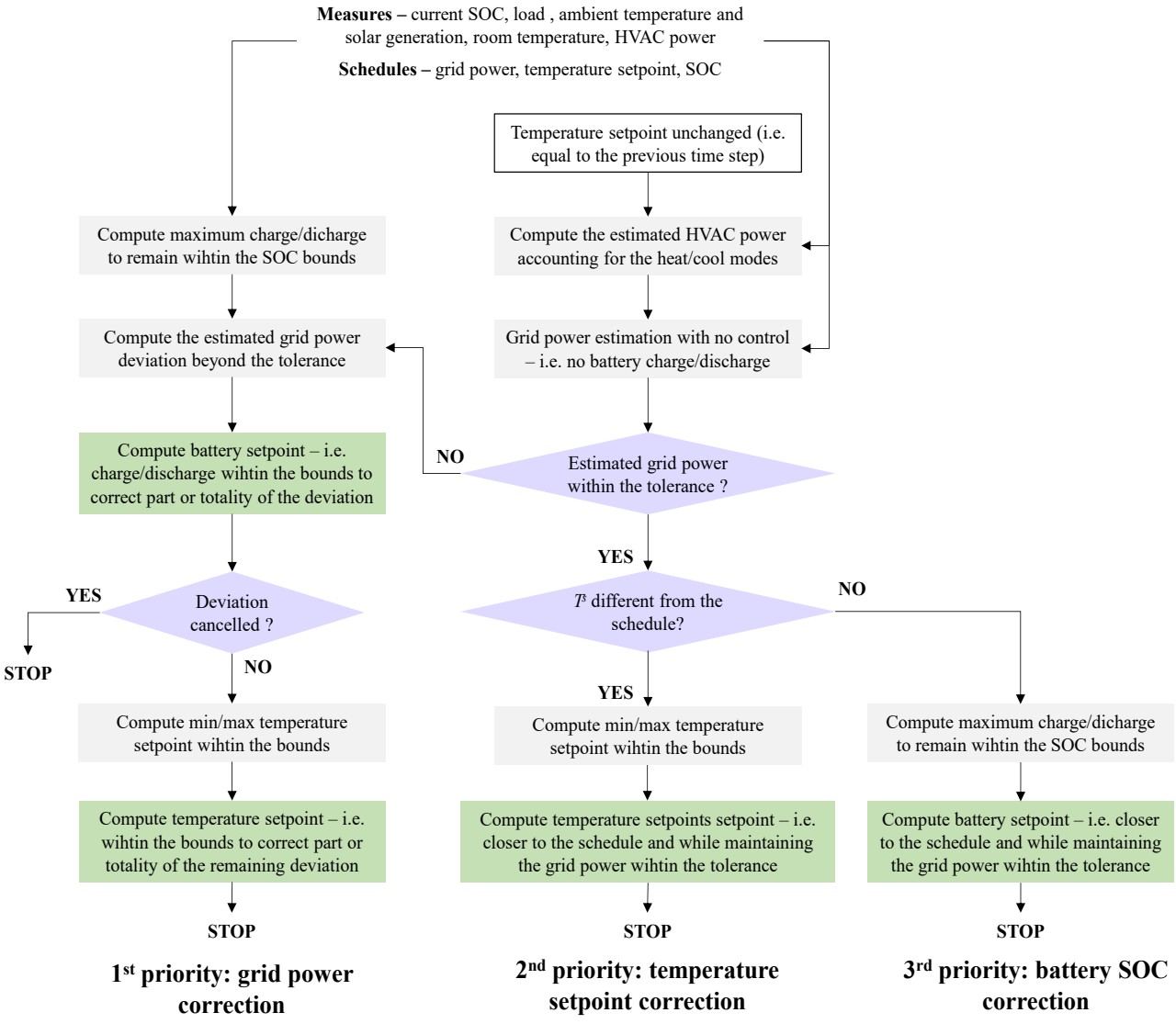

Figure 6: Flowchart of the implemented RBC

The flowchart of the considered RBC is displayed in Figure 6. For the sake of clarity, equations in the test blocks and calculation of the control values are not explicitly described. The underlying idea is to stick to the logic implicitly represented in the optimization problem introduced in the previous subsection. Overall, the priority is to maintain the grid power profile within the tolerance bandwidth (Δp^{gd}). To do so, the battery is firstly used within its own bounds – i.e. maximum charge/discharge and accounting for the SOC tolerance (Δsoc). If the battery action is not enough to compensate for the grid power deviation from the scheduled profile, then the temperature setpoint is tuned within its bounds (min/max values and accounting for the maximum variation ΔT^{s}). Otherwise, if at a given time step forecast errors are not significant, the estimated grid power value (with no controls) may be within the tolerance bandwidth. That bandwidth is then used as a degree of freedom to correct if needed, the temperature setpoint according to the scheduled values. If the setpoint matches the schedule, the charge/discharge of the battery is adapted to bring the SOC closer to the predicted value. Obviously, those last two actions, shall not lead to a grid power beyond the tolerance. The larger the bandwidth in the near real-time control, the larger the degree of freedom to adjust temperature setpoints and SOC. The settings of the real-time control parameter will be discussed in Section 3.2.

3.6 Performance Metrics

Two criteria are defined to assess the performances of the proposed control methodology and represent the two main target objectives – *i)* power profile smoothing and *ii)* predictability. The first metric denoted E^2 is somewhat homogeneous to the square of the energy exchanged with the grid (i.e. import/export) in kW^2. It represents the capacity to smoothen the grid power profile with the objective targeted in the look-ahead phase (Eq. (28)). The second criterion E^{dev} in kW estimates the total energy contained in power deviations around the committed grid power profile and tolerance bandwidth (Eq. (29)).

$$E^2 = \sum_{t \in T} \left(p_t^{gd} \right)^2 \times dt \tag{28}$$

$$E^{dev} = \delta^+ + \delta^- \text{ with } \begin{cases} \delta^+ = p_t^{gd} - \left(p_t^{gd*} + \Delta p^{gd} \right) & \text{if } p_t^{gd} > \left(p_t^{gd*} + \Delta p^{gd} \right) \\ \delta^- = \left(p_t^{gd*} - \Delta p^{gd} \right) - p_t^{gd} & \text{if } p_t^{gd} < \left(p_t^{gd*} - \Delta p^{gd} \right) \end{cases} \tag{29}$$

4 Obtained Results and Sensitivity Analysis

This section presents the obtained results over different test periods and for different parameters tuning of the real-time controller. Load profiles [32] and weather data [33] (temperature and solar radiation) are considered over a full year at a sampling resolution of 5 min for the system simulation in near real-time operations. In the look-ahead MPC, at first, and in order to emulate the forecast 'lack of accuracy', the predictions for a given day (load, temperature, and solar generation) are generated using the profiles of the previous days, resampled at 30 min. The installed solar panel and battery storage have capacities of 3 kWp and 3 kWh, respectively.

4.1 Results Over a Single Day

A first daily simulation (summer day) is performed for a summer day. The parameters for the real-time MPC are set to: Δp^{gd} = 300 W, Δsoc = 50 %, and ΔT = 0.5°C. Obtained results are displayed in Figure 7. Especially, Figure 7a displays the grid power profiles with the day-ahead commitment to follow and the tolerance bandwidth (Δp^{gd} = 300 W here). It also highlights the interest of real-time controls that allow to remain within that tolerance most of the time, compared to a case in which the controls scheduled on the look-ahead phase remain unchanged (grey curve). In case of a potential generation deficit compared to the forecasts, the net grid power may exceed the predicted (point **A**) if the controls scheduled on the look-ahead phase are not corrected. However, it is mitigated thanks to the near real-time MPC with a battery discharge while the state of charge remains within the tolerance bandwidth (Δsoc = 50 % here) around the scheduled patterns (Figure 7b). When there is a generation surplus or an electrical load level lower than predictions (point **B**), the solution considered in real-time for the simulated day comprises increasing the cooling power by reducing the temperature setpoint (Figure 7c).

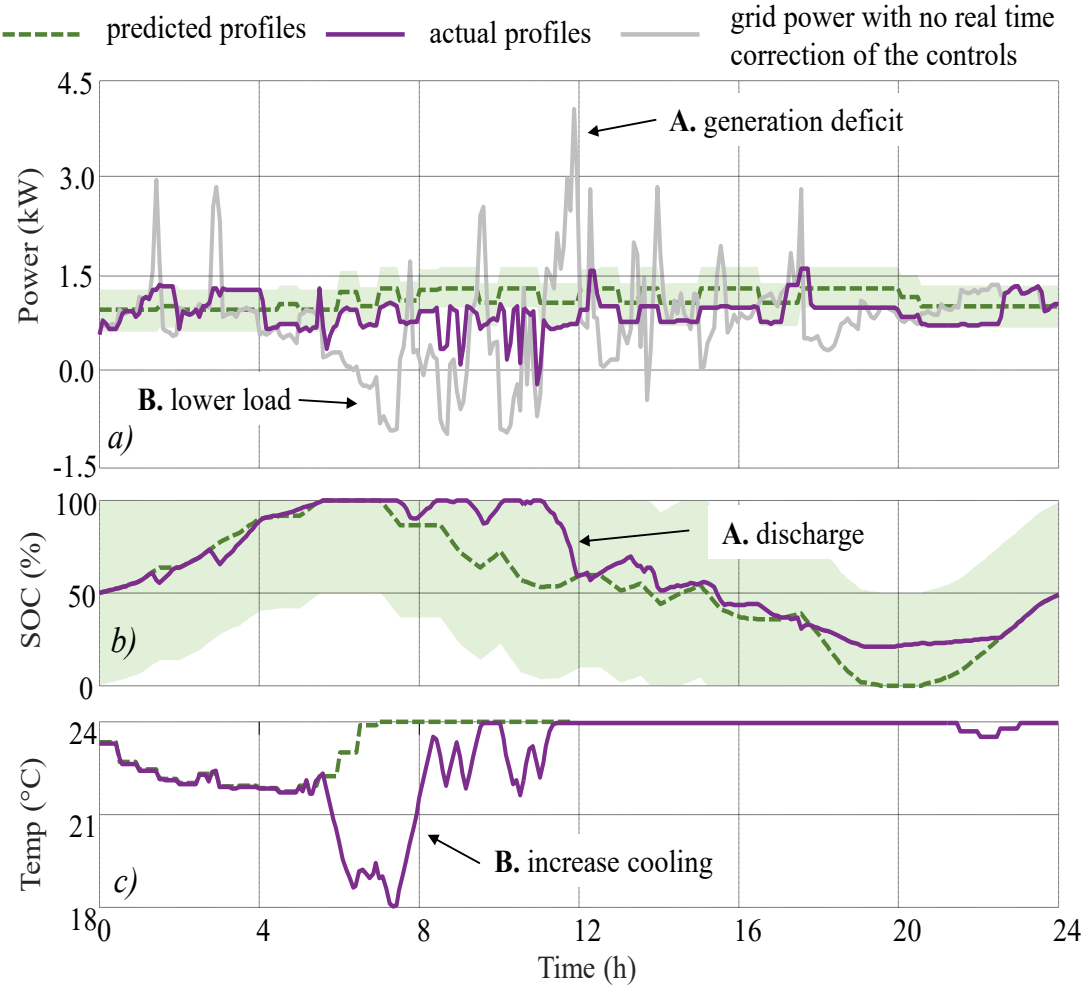

Figure 7: Results for a single summer day – a) grid power profile – b) state of charge – c) temperature setpoint.

Table 1 displays the values obtained for the two considered metrics over four different days (seasonal). The case without control does not consider any battery and temperature setpoints adjustment. In that case, the prediction of the grid power is purely based on solar generation and an estimation of the cooling/heating load with a temperature setpoint at 21°C and the forecasted ambient temperature. Results highlight the need for real-time adaptation of the control, especially for uncertainties mitigation and to remain closer to the predicted commitment. Best values for both objectives are obtained with the proposed approach with the online tuning of the thermal model (at 5 min resolution). Note that both MPC and RBC approaches for the near real-time management alternatively returns best values for one of the two metrics.

Table 1: Power profile smoothing and predictability metrics for four different simulation days

	Winter		Spring		Summer		Autumn	
	E^2	E^{dev}	E^2	E^{dev}	E^2	E^{dev}	E^2	E^{dev}
No control, no MPC	164.5	9.6	116.1	20.4	46.6	17.6	66.5	11.14
Look-ahead MPC, no real-time control	104.6	5.8	73.1	14.6	27.4	9.19	33.9	6.9
Look-ahead and real-time MPC	121.9	3.5	111.4	5.6	25.6	1.3	34.7	2.5
Look-ahead and real-time MPC, model tuning	**100.0**	**0.7**	**82.9**	2.3	**20.3**	0.9	26.8	**0.8**
Look-ahead MPC and real-time RBC, model tuning	101.6	1.9	88.8	**1.7**	21.0	**0.4**	**20.6**	1.2

Note that simulations were performed on an Intel Core i5 @ 1.6 GHz, 16GB RAM. The computational burden is very light. The considered Mixed Integer Quadratic Programming (MIQP) problems are solved with Gurobi 10.0.0. The look-ahead stage takes on average 2.21 seconds to run, while the near real-time optimization is performed on average in 0.73 seconds.

4.2 Impact of the Near Real-Time Control Parameters

In the second stage, the proposed approach is run over four days (one per season) and with different sets of parameter values for the near real-time MPC. Obtained results are displayed in Figure 8 with the two metrics (energy exchanges E^2 and deviation from commitment E^{dev}) summed along the four days and plotted in every case. Obviously, deviations around the committed grid profile are maximum when no tolerance bandwidth is considered (Δp^{gd} = 0 W in Figure 8a). At the same time, oscillations around the committed profile are reduced, this also tends to decrease the overall indicator on the energy exchanges E^2 with a smoother grid profile. Also, the bigger the tolerance bandwidth around the scheduled SOC profiles, the bigger the available capacity in real-time to mitigate uncertainties (i.e. more reserve), and the smaller the deviation and smoother the grid profiles (Δsoc = 50 % in Figure 8b). The ramping limit of the temperature setpoints between two successive time steps appears to have no impact on the energy exchanges (E^2). However, bigger ramping limits slightly reduce the deviations around the commitment while providing more degrees of freedom in the real-time correction (Δsoc = 50 % in Figure 8b).

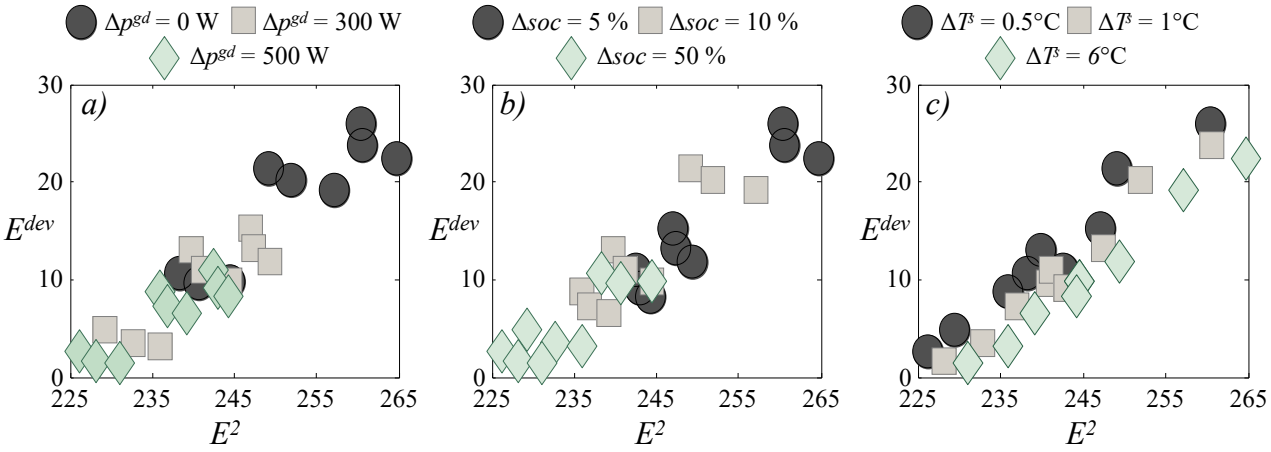

Figure 8: Controller performances over four distinct seasonal days – a) Δp^{gd} – b) Δsoc = 50 % – c) ΔT^s

Table 2 summarizes four settings extracted from the investigated scenarios that displayed the best performances for both MPC and RBC methods for near real-time management. Overall, performances returned by the MPC approach are slightly better than the ones from the rule-based method. However, in the following section several runs of the control strategy will be performed, and the RBC is applied to reach a shorter computational time.

Table 2: Parameters settings returning the best performances over the four seasonal days.

			Look-ahead and real-time MPC, model tuning		Look-ahead MPC and real-time RBC, model tuning	
Δp^{gd}	Δsoc	ΔT^s	E^2	E^{dev}	E^2	E^{dev}
300 W	50 %	0.5°C	229.1	4.7	231.5	5.2
300 W	50 %	1.0°C	229.1	1.6	238.1	5.0
500 W	50 %	0.5°C	226.2	2.6	239.13	7.55
500 W	50 %	1.0°C	229.1	1.6	241.7	6.3

4.3 Trade-Off Between System Performances and Battery Usage

Previous simulations and modeling neglected any impact of battery usage on its degradation and cost. In practice, any over usage (e.g. higher rates of charge/discharge currents, numbers of cycles) along with severe environmental conditions can significantly impact the storage lifespan. In the field of power and energy systems

management and planning, conventional problems approximate battery degradation with simplified linear/convex models [34], [35] – even though nonlinear representations based on more accurate battery models [17] or cycle counting algorithms [36] can be found. Especially, at the first order, aging is characterized by a loss of storage capacity over time that is dependent on the energy exchanged along the simulated horizon (i.e. the integration of charging/discharging power over time) [37]. Deriving from simple linear models, this subsection then introduces a degradation metric in terms of the 'number of equivalent cycles' – i.e. the exchanged energy divided by the nominal capacity of the battery. This metric is integrated as a constraint in the first look-ahead stage of the MPC where a maximum number of cycles per day N_{cycle_max} is set ((30)). Especially, a factor α in [0,1] is introduced in order to allow more or less battery usage. Similarly, for the near real-time stage, the factor α is used to set the maximum battery power available for uncertainties mitigation ((31)).

$$\frac{\sum_{t\in T}\left(p_t^{bat+}+p_t^{bat-}\right)\times dt}{2\times\overline{e^{bat}}}\leq(1-\alpha)\times N_{cycle\_\max} \tag{30}$$

$$\overline{p^{bat}}\leftarrow(1-\alpha)\times\overline{p^{bat}} \tag{31}$$

There is then a trade-off between the system performances and the battery usage – no usage at all for α = 0. A new set of simulations is performed while varying the allowed battery usage along the four tested days (one per season). Note that there is no cost consideration or long-term sizing perspective in the paper that focuses mainly on operation planning. Thus, battery usage is not used here to assess the economic viability of the system or to account for the loss of storage capacity over time. Instead, a degradation indicator in terms of 'the number of equivalent cycles is analyzed with regards to its impact on the technical performance metrics – i.e. energy exchanges E^2 and energy deviation with commitment E^{dev}. Obtained results are displayed in Figure 9 where performance metrics display their worst value when the battery is not used at all. In such a case the only degree of control for the building comes from temperature setpoint tuning. Most significant improvements, especially in terms of energy exchanges, occur whit greater batter usages over four equivalent cycles. Thus, a conservative approach to estimate the battery degradation for that kind of application is to assess roughly one daily cycle (simulations performance along four test days).

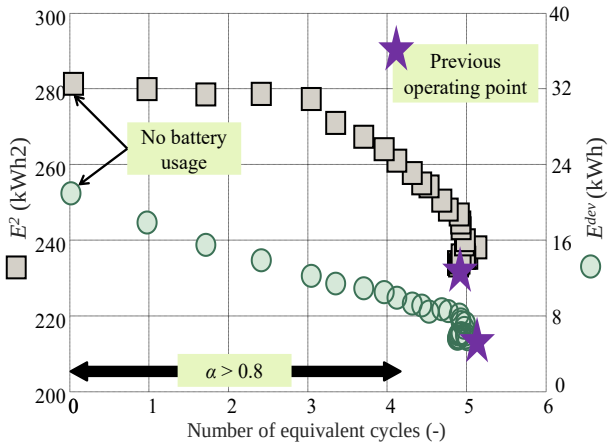

Figure 9: System performance metrics (E^2 and E^{dev} to minimize) versus battery usage along four test days

4.4 Cross Sensitivity of the Forecast Accuracy and Storage Size

In this subsection additional simulations are performed while assessing different forecast quality – for the electrical load (p_t^l), solar radiation (G_t), and temperature (T_t^a). As illustrated in Appendix, forecast profiles for each four seasonal days are taken from historical profiles during the same year. The idea is to assess the impact of the forecast quality and storage capacity (in the range 0 kWh – 10 kWh). Note that the solar panel peak power remains fixed here at 3 kWp. Simulations are then performed with different battery capacities and three distinct forecast qualities. Results are displayed in Figure 10, which are computed (mean and confidence interval at 95%) over twenty independent runs in every case – with different forecast profiles at every run. Obviously, the greater

the installed capacity, the more reduced the grid exchanges over the tested day, no matter the forecast quality – i.e. decreasing E^2 in Figure 10*a*. Note that with a value of 456 kWh^2 for the baseline scenarios (i.e. no storage, no thermal control), gains are significant over 25 % in every case – almost half of it allowed by the thermal control (i.e. no storage in Figure 10*a*). Also, with bad forecast quality, it tends to be more difficult to stick to the committed grid profile as displayed in Figure 10*b* with near constant E^{dev} with varying installed battery capacity. In addition to the energy deviation with the commitment, it is worth estimating the error between the predicted grid exchanges and the actual ones (E^2). Figure 10*c* displays this error (MAE in %) and confidence interval over twenty independent runs. As for E^{dev}, the accuracy of the forecast significantly affects this error. It is worth noticing that the error also increases with the installed battery capacity. It can be somewhat counterintuitive as more capacity would provide more degree of freedom to absorb deviations between actual and forecasted values. However, in the look-ahead stage, the battery capacity is used in a scheduling phase to smooth the grid power profile (expected for the next day) as much as possible. This leads to an optimal schedule of the battery that oscillates between its minimum/maximum *soc* values for energy arbitrage purposes – at 30 min resolution forecast. Assuming that the battery can follow its schedule in real-time and reach lower state of charge values at a given time step, it would not be able to absorb a sudden deficit of local generation (e.g. important load and/or cooling/heating needs, lower solar generation).

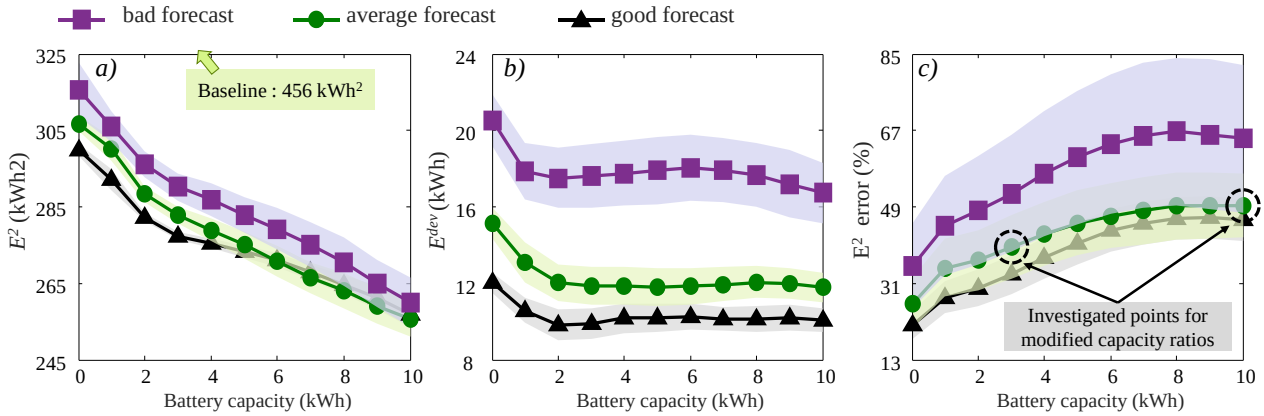

Figure 10: Mean results and confidence interval at 95 % over 20 independent runs for different forecast quality and battery capacity – a) grid exchanges E^2 -b) deviations around the commitment E^{dev} – c) mean error between predicted and actual grid exchanges E^2.

Following the previous observations, a last set of simulations/tests is performed while considering the average forecast quality for two different battery capacities 3 kWh and 10 kWh – highlighted points in Figure 10*c*. Different scenarios are considered while varying the amount of battery capacity that is reserved in day-ahead operations. A capacity ratio is then defined in the range of 0 – 50 % to account for more or less capacity available in the look-ahead optimization. Concretely, an allowed state of charge bandwidth around 50 % is implemented while adjusting the SOC constraints in the optimization problem (Eq. (6)) – e.g. ± 10 % around 50 %, ± 20 %, ± 30 %, etc. Results presented over the three charts in Figure 11 highlight the trade-off between actual and deviations from the predictions. As previously observed, increased battery capacity reduces the actual grid exchanges (Figure 11a). However, the improvement rate decreases with greater capacity ratios in look-ahead optimization – i.e. decreasing slope in Figure 11a. At the same time, increased capacity ratios lead to more deviations with the commitment – both in energy (Figure 11b) and while comparing the actual grid exchanges with the predicted ones (Figure 11c). An interesting trade-off is identified for the investigated capacities around 10 – 20 % of the overall storage is usable in the day-ahead phase.

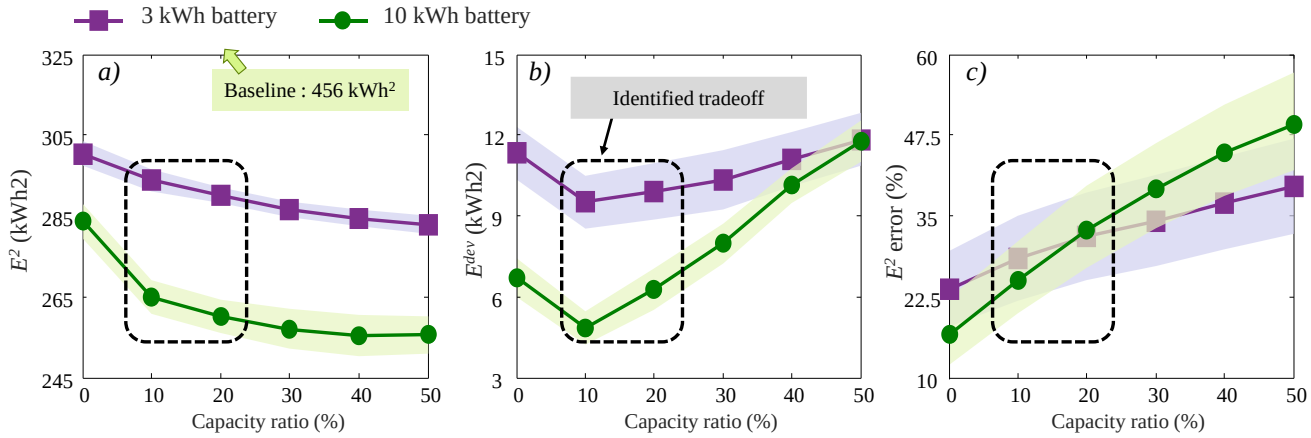

Figure 11: Mean results and confidence interval at 95 % over 20 independent runs for different battery capacity and usable capacity ratio – a) grid exchanges E^2 -b) deviations around the commitment E^{dev} – c) mean error between predicted and actual grid exchanges E^2.

5 Conclusions

In this manuscript, a two-stage energy management was proposed that mitigates both forecast uncertainties and model equations approximations in model-based controllers. The first MILP stage minimizes the predicted exchanges with the grid and generates a daily energy commitment profile. This committed profile is then used as a reference for the near real-time controller (both optimization and rule-based approaches were tested). The proposed strategy adapts the system model in real-time based on the uncertain solar generation, demand, and ambient temperature. In addition, performances of the real-time control are enhanced while tuning online the model used in the decision-making process with the observed deviations at the previous time steps. This is allowed with the consideration of different model granularities in both the first and second stage controller compared to a reference building representation to which the controls are sent. Simulations performed show that the energy management strategy follows the predicted/committed grid profile with small deviations in real-time operation. The simulations conducted under different weather conditions demonstrated that the proposed strategy reduces energy exchange by at least 25% while meeting the household's energy demand and comfort requirements. Furthermore, sensitivity analysis of the forecast quality and battery capacity was also presented to derive a crucial understanding. Ongoing additional works investigate the possibility to control clusters of building with the implementation of coordination/decentralization schemes. The objective is to uptake higher performance and take advantage of heterogenous energy usages to further enhance the integration of renewable sources with higher systems predictability.

6 Acknowledgments

This work has been carried out in the framework of the INT2MEC project - INTelligent Multi-Energy Communities for enhanced distributed resources INTegration in Singapore. The research is supported by the National Research Foundation, Prime Minister'sOffice, Singapore under its Campus for Research Excellence and Technological Enterprise (CREATE) program.

7 References

[1] S. Farooq and W. ul Zahoor, 'Smart grid-energizing towards a greener future', in *2015 Power Generation System and Renewable Energy Technologies (PGSRET)*, Jun. 2015, pp. 1–5. doi: 10.1109/PGSRET.2015.7312184.

[2] M. Vasiliev, M. Nur-E-Alam, and K. Alameh, 'Recent Developments in Solar Energy-Harvesting Technologies for Building Integration and Distributed Energy Generation', *Energies*, vol. 12, no. 6, p. 1080, Jan. 2019, doi: 10.3390/en12061080.

[3] A.-L. Klingler, 'Self-consumption with PV+Battery systems: A market diffusion model considering individual consumer behaviour and preferences', *Applied Energy*, vol. 205, pp. 1560–1570, Nov. 2017, doi: 10.1016/j.apenergy.2017.08.159.

[4] J. Zupančič, B. Filipič, and M. Gams, 'Genetic-programming-based multi-objective optimization of strategies for home energy-management systems', *Energy*, vol. 203, p. 117769, Jul. 2020, doi: 10.1016/j.energy.2020.117769.

[5] S. Sharma, A. Verma, Y. Xu, and B. K. Panigrahi, 'Robustly Coordinated Bi-Level Energy Management of a Multi-Energy Building Under Multiple Uncertainties', *IEEE Transactions on Sustainable Energy*, vol. 12, no. 1, pp. 3–13, Jan. 2021, doi: 10.1109/TSTE.2019.2962826.

[6] J. K. Gruber and M. Prodanovic, 'Two-stage Optimization for Building Energy Management', *Energy Procedia*, vol. 62, pp. 346–354, 2014, doi: 10.1016/j.egypro.2014.12.396.

[7] T. H. B. Huy, H. T. Dinh, and D. Kim, 'Multi-objective framework for a home energy management system with the integration of solar energy and an electric vehicle using an augmented ε-constraint method and lexicographic optimization', *Sustainable Cities and Society*, vol. 88, p. 104289, Jan. 2023, doi: 10.1016/j.scs.2022.104289.

[8] U. Mir, U. Abbasi, T. Mir, S. Kanwal, and S. Alamri, 'Energy Management in Smart Buildings and Homes: Current Approaches, a Hypothetical Solution, and Open Issues and Challenges', *IEEE Access*, vol. 9, pp. 94132–94148, 2021, doi: 10.1109/ACCESS.2021.3092304.

[9] A. C. Duman, H. S. Erden, Ö. Gönül, and Ö. Güler, 'A home energy management system with an integrated smart thermostat for demand response in smart grids', *Sustainable Cities and Society*, vol. 65, p. 102639, Feb. 2021, doi: 10.1016/j.scs.2020.102639.

[10] S. S. Ghayour and T. Barforoushi, 'Optimal scheduling of electrical and thermal resources and appliances in a smart home under uncertainty', *Energy*, vol. 261, p. 125292, Dec. 2022, doi: 10.1016/j.energy.2022.125292.

[11] M. H. Dadashi-Rad, A. Ghasemi-Marzbali, and R. A. Ahangar, 'Modeling and planning of smart buildings energy in power system considering demand response', *Energy*, vol. 213, p. 118770, Dec. 2020, doi: 10.1016/j.energy.2020.118770.

[12] J. Zupančič, B. Filipič, and M. Gams, 'Genetic-programming-based multi-objective optimization of strategies for home energy-management systems', *Energy*, vol. 203, p. 117769, Jul. 2020, doi: 10.1016/j.energy.2020.117769.

[13] S. A. Mansouri, A. Ahmarinejad, E. Nematbakhsh, M. S. Javadi, A. R. Jordehi, and J. P. S. Catalão, 'Energy management in microgrids including smart homes: A multi-objective approach', *Sustainable Cities and Society*, vol. 69, p. 102852, Jun. 2021, doi: 10.1016/j.scs.2021.102852.

[14] S. Zamanloo, H. Askarian Abyaneh, H. Nafisi, and M. Azizi, 'Optimal two-level active and reactive energy management of residential appliances in smart homes', *Sustainable Cities and Society*, vol. 71, p. 102972, Aug. 2021, doi: 10.1016/j.scs.2021.102972.

[15] S. Sharma, Y. Xu, A. Verma, and B. K. Panigrahi, 'Time-Coordinated Multienergy Management of Smart Buildings Under Uncertainties', *IEEE Transactions on Industrial Informatics*, vol. 15, no. 8, pp. 4788–4798, Aug. 2019, doi: 10.1109/TII.2019.2901120.

[16] A. Anvari-Moghaddam, H. Monsef, and A. Rahimi-Kian, 'Optimal Smart Home Energy Management Considering Energy Saving and a Comfortable Lifestyle', *IEEE Transactions on Smart Grid*, vol. 6, no. 1, pp. 324–332, Jan. 2015, doi: 10.1109/TSG.2014.2349352.

[17] Y. Li, D. M. Vilathgamuwa, D. E. Quevedo, C. F. Lee, and C. Zou, 'Ensemble Nonlinear Model Predictive Control for Residential Solar–Battery Energy Management', https://doi.org/10.48550/arXiv.2303.10393

[18] M. Gholamzadehmir, C. Del Pero, S. Buffa, R. Fedrizzi, and N. Aste, 'Adaptive-predictive control strategy for HVAC systems in smart buildings – A review', *Sustainable Cities and Society*, vol. 63, p. 102480, Dec. 2020, doi: 10.1016/j.scs.2020.102480.

[19] R. Rigo-Mariani, B. Sareni, X. Roboam, S. Astier, E. Cahuet, and J.-G. Steinmetz, 'Off-line and On-line Power Dispatching Strategies for a Grid Connected Commercial Building with Storage Unit', *IFAC Proceedings Volumes*, vol. 45, no. 21, pp. 266–271, 2012, doi: 10.3182/20120902-4-FR-2032.00048.

[20] S. Aznavi, P. Fajri, A. Asrari, and J. Khazaei, 'Two-Stage Energy Management of Smart Homes in Presence of Intermittencies', in *2019 IEEE Transportation Electrification Conference and Expo (ITEC)*, Jun. 2019, pp. 1–5. doi: 10.1109/ITEC.2019.8790479.

[21] 'Two-stage Optimization for Building Energy Management', *Energy Procedia*, vol. 62, pp. 346–354, 2014, doi: 10.1016/j.egypro.2014.12.396.

[22] M. C. Di Piazza, G. La Tona, M. Luna, and A. Di Piazza, 'A two-stage Energy Management System for smart buildings reducing the impact of demand uncertainty', *Energy and Buildings*, vol. 139, pp. 1–9, Mar. 2017, doi: 10.1016/j.enbuild.2017.01.003.

[23] G. Pinto, D. Deltetto, and A. Capozzoli, 'Data-driven district energy management with surrogate models and deep reinforcement learning', *Applied Energy*, vol. 304, p. 117642, Dec. 2021, doi: 10.1016/j.apenergy.2021.117642.

[24] J. Wang, S. Li, H. Chen, Y. Yuan, and Y. Huang, 'Data-driven model predictive control for building climate control: Three case studies on different buildings', *Building and Environment*, vol. 160, p. 106204, Aug. 2019, doi: 10.1016/j.buildenv.2019.106204.

[25] M. D. Knudsen and S. Petersen, 'Economic model predictive control of space heating and dynamic solar shading', *Energy and Buildings*, vol. 209, p. 109661, Feb. 2020, doi: 10.1016/j.enbuild.2019.109661.

[26] D. Wang, Y. Chen, W. Wang, C. Gao, and Z. Wang, 'Field test of Model Predictive Control in residential buildings for utility cost savings', *Energy and Buildings*, vol. 288, p. 113026, Jun. 2023, doi: 10.1016/j.enbuild.2023.113026.

[27] I. L. R. Gomes, M. G. Ruano, and A. E. Ruano, 'MILP-based model predictive control for home energy management systems: A real case study in Algarve, Portugal', *Energy and Buildings*, vol. 281, p. 112774, Feb. 2023, doi: 10.1016/j.enbuild.2023.112774.

[28] S. Shongwe and M. Hanif, 'Comparative Analysis of Different Single-Diode PV Modeling Methods', *IEEE Journal of Photovoltaics*, vol. 5, no. 3, pp. 938–946, May 2015, doi: 10.1109/JPHOTOV.2015.2395137.

[29] S. Troitzsch, kaiATtum, tomschelo, and arifa7med, *mesmo-dev/mesmo:* Zenodo, 2021. Accessed: Apr. 11, 2023. [Online]. Available: https://zenodo.org/record/5674243

[30] J. Zhu, *Optimization of Power System Operation*. John Wiley & Sons, 2015.

[31] J. Lofberg, 'YALMIP : a toolbox for modeling and optimization in MATLAB', in *2004 IEEE International Conference on Robotics and Automation (IEEE Cat. No.04CH37508)*, Sep. 2004, pp. 284–289. doi: 10.1109/CACSD.2004.1393890.

[32] D. Murray, L. Stankovic, and V. Stankovic, 'An electrical load measurements dataset of United Kingdom households from a two-year longitudinal study', *Sci Data*, vol. 4, no. 1, p. 160122, Jan. 2017, doi: 10.1038/sdata.2016.122.

[33] 'U.S. Climate Reference Network after One Decade of Operations: Status and Assessment in: Bulletin of the American Meteorological Society Volume 94 Issue 4 (2013)'. https://journals-ametsoc-org.sid2nomade-1.grenet.fr/view/journals/bams/94/4/bams-d-12-00170.1.xml (accessed Apr. 11, 2023).

[34] B. Li, R. Roche, D. Paire, and A. Miraoui, 'Sizing of a stand-alone microgrid considering electric power, cooling/heating, hydrogen loads and hydrogen storage degradation', *Applied Energy*, vol. 205, pp. 1244–1259, Nov. 2017, doi: 10.1016/j.apenergy.2017.08.142.

[35] G. Cardoso, T. Brouhard, N. DeForest, D. Wang, M. Heleno, and L. Kotzur, 'Battery aging in multi-energy microgrid design using mixed integer linear programming', *Applied Energy*, vol. 231, pp. 1059–1069, Dec. 2018, doi: 10.1016/j.apenergy.2018.09.185.

[36] M. A. Hossain, H. R. Pota, S. Squartini, F. Zaman, and J. M. Guerrero, 'Energy scheduling of community microgrid with battery cost using particle swarm optimisation', *Applied Energy*, vol. 254, p. 113723, Nov. 2019, doi: 10.1016/j.apenergy.2019.113723.

[37] P. V. H. Seger, R. Rigo-Mariani, P.-X. Thivel, and D. Riu, 'A storage degradation model of Li-ion batteries to integrate ageing effects in the optimal management and design of an isolated microgrid', *Applied Energy*, vol. 333, p. 120584, Mar. 2023, doi: 10.1016/j.apenergy.2022.120584.

[38] F. Lazzeri, *Machine Learning for Time Series Forecasting with Python*. John Wiley & Sons, 2020.

[39] I. Kim and W. Kim, 'Application of market-based control with thermal energy storage system for demand limiting and real-time pricing control', *Energy*, vol. 263, p. 125579, Jan. 2023, doi: 10.1016/j.energy.2022.125579.

[40] Y. Ye, D. Qiu, X. Wu, G. Strbac, and J. Ward, 'Model-Free Real-Time Autonomous Control for a Residential Multi-Energy System Using Deep Reinforcement Learning', *IEEE Transactions on Smart Grid*, vol. 11, no. 4, pp. 3068–3082, Jul. 2020, doi: 10.1109/TSG.2020.2976771.

[41] Y. Gao, S. Li, X. Fu, W. Dong, B. Lu, and Z. Li, 'Energy management and demand response with intelligent learning for multi-thermal-zone buildings', *Energy*, vol. 210, p. 118411, Nov. 2020, doi: 10.1016/j.energy.2020.118411.

8 Appendix A

The last sets of simulations performed in this manuscript relies on various forecast for the four seasonal days considered. The forecasts refer to the predicted day-ahead profiles for the solar radiation, ambient temperature, and electrical load. As presented in the manuscript those profiles are input of the look-ahead MPC that allows to define the schedules before real-time control is applied. More specifically, the idea in Section 3.3 is to assess the impact of the forecast quality. Thus, for every investigated day, several forecast profiles shall be generated with different degree of accuracy. In the absence of historical forecasts, a most rigorous approach could consist of implementing different time series predictors [38] and train them to reach distinct degree of accuracy – e.g. while reducing the training set and/or training iterations. However, the development of such forecasting tools is beyond the scope of the paper. Thus, for the sake of simplicity, forecasts are here taken from historical data along the same year as the four seasonal reference days. For each of those reference days, the other daily profiles are arranged in ascending order with regards to the error compared to the daily reference. The error is the RMSE normalized by the standard deviation of the reference daily power – i.e. a RMSE of 100 % denotes a forecast that displays as much variations around the actual values as the natural variation of the reference profiles around its mean values. Figure 12 displays sets of twenty forecast profiles of different quality (four different quality in columns) for the load (1st row), temperature (2nd row) and solar radiation (3rd row). The most accurate prediction for the solar radiation and temperature reaches RMSE values of 20-40%. However, the load profile at the scale of a single household being much noisier and with less deterministic seasonality/daily variations, the lowest RMSE values observed are above 70 %.

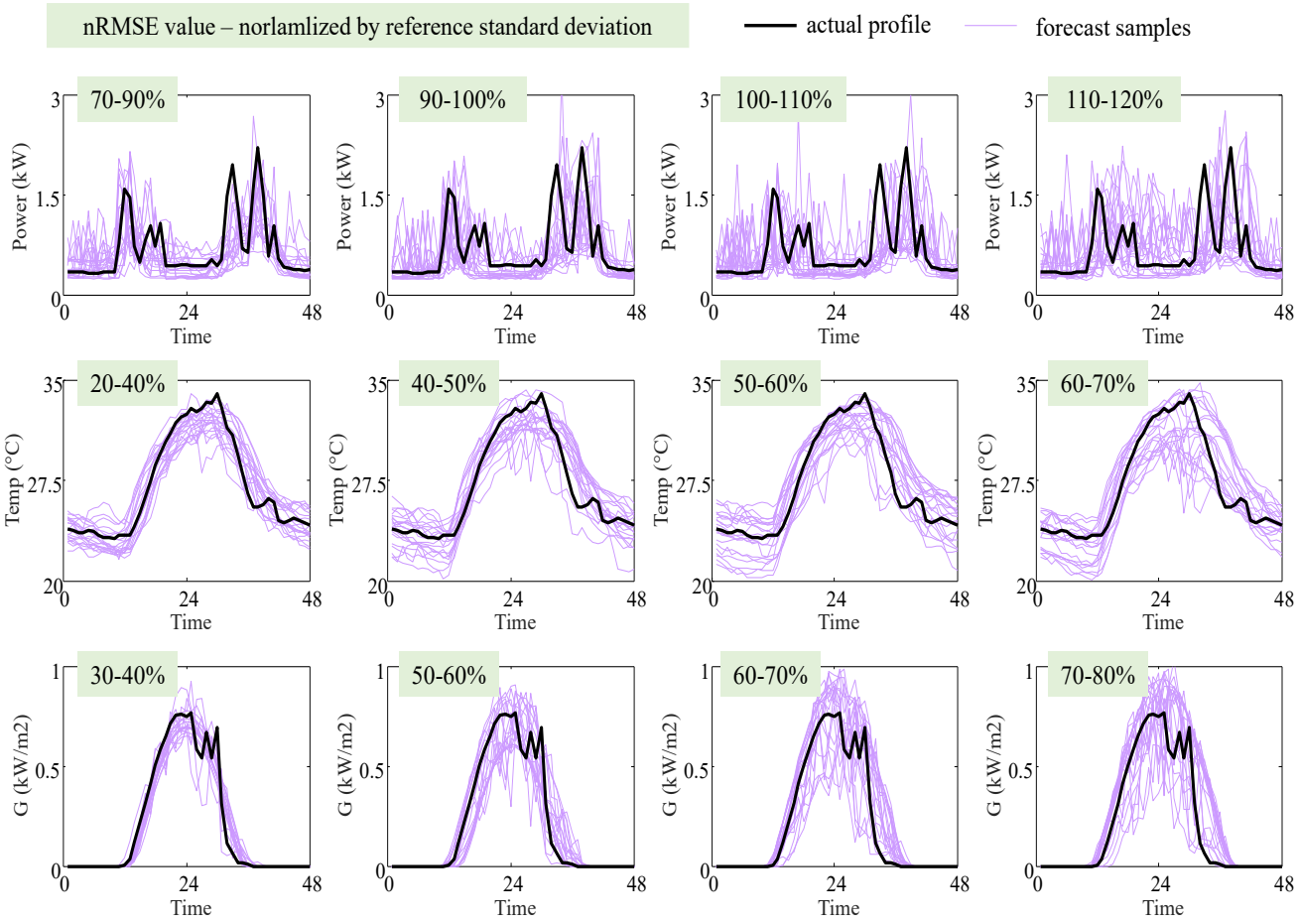

Figure 12: Sample forecasts for the reference day in autumn – different forecast quality for the load, ambient temperature and solar radiation profiles.

9 Appendix B

Table 3 summarizes the short literature review performed to highlight the scope of the proposed paper.

Table 3: Parameters settings returning the best performances over the four seasonal days.

Ref.	Case Study, DERs and controls	Objectives	Controller Algorithm	HVAC Model	Two-Stage Strategy	Validation Model/System
[7]	Single house, PV, EV, storage, HVAC	Cost, PAR	MILP	✓		
[10]	Single house, multi-energy, PV, thermal/electrical storages, controllable loads	Cost	MILP			
[11]	Multiple houses in a distribution grid, PV, storage, controllable loads	Cost	PSO			
[12]	Single house, PV, storage	Cost, emissions	GA			
[19]	Single building, PV, storage	Cost	NLP and heuristic		✓	
[39]	Single house, PV, storage, controllable load	Cost, energy	DP and heuristic			✓
[13]	Multiple houses in a distribution grid, PV, storage, controllable load	Cost, emissions, PAR	MIQCP			
[15]	Single house, multi-energy, PV, thermal/electrical storages, controllable loads	Cost	MINLP		✓	
[14]	Single household, PV, storage, controllable loads	Cost	MILP	✓		
[16]	Single house, multi-energy, PV, fuel cell, storage, CHP unit	Cost	MINLP	✓		
[9]	Single house, multi-energy, PV, thermal/electrical storages, controllable loads	Cost	MILP	✓		
[22]	Single house, PV, Storage	Cost	MILP / DP		✓	
[20]	Single house, PV, EV, storage, controllable loads	Costs	Metaheuristic		✓	
[5]	Single house, multi-energy, PV, fuels cell, storage, CHP unit	Costs	MINLP	✓	✓	
[21]	Single house, PV, storage, controllable loads	Cost	MILP		✓	
[40]	Single house, multi energy, PV, storage	Cost	RL			
[23]	Multiple buildings, PV, storage	Cost	RL	✓		✓
[24]	Single building	Cost	RL	✓		✓
[41]	Single building, controllable load	Cost	PSO	✓		✓
[26]	Single house	Cost	NLP	✓		✓
[27]	Single building, storage	Cost	MILP	✓		✓
[25]	Single building	Cost	MILP	✓		✓
This work	**Single house, PV, storage**	**Energy exchanges**	**MILP/QP and heuristic**	✓	✓	✓

PV : photovoltaics, EV : electrical vehicles, MILP : mixed integer linear programming, MIQP : mixed integer quadratic programming, PSO : particle swarm optimization, GA : genetic algorithm, PAR : peak to average ratio, MIQCP : mixed integer quadratically constrained programming, CHP : combined heat and power, NLP : nonlinear programming, MINLP : mixed integer nonlinear programming, DP : dynamic programming, RL : reinforcement learning